







Three-stage laser cooling of Sr atoms using the $5s5p\ ^3P_2$ metastable state below Doppler temperatures

Tomoya Akatsuka ^{1,2,*} Koji Hashiguchi ^{1,2,†} Tadahiro Takahashi ^{1,2} Noriaki Ohmae ^{1,2}
Masao Takamoto ² and Hidetoshi Katori ^{1,2}

¹*Department of Applied Physics, Graduate School of Engineering, The University of Tokyo, Bunkyo-ku, Tokyo 113-8656, Japan*

²*Quantum Metrology Laboratory, RIKEN, Wako, Saitama 351-0198, Japan*



(Received 12 December 2020; accepted 8 February 2021; published 25 February 2021)

We report three-stage laser cooling of Sr atoms using the $5s^2\ ^1S_0$ ground state and the $5s5p\ ^3P_2$ metastable state. ^{87}Sr atoms are precooled in a magneto-optical trap simultaneously operated on the $5s^2\ ^1S_0$ – $5s5p\ ^1P_1$ transition at 461 nm and on the $5s5p\ ^3P_2$ – $5s5d\ ^3D_3$ transition at 496 nm. Atoms optically pumped to the $5s5p\ ^3P_2$ ($F = 13/2$) state are magneto-optically trapped and cooled down to $2.5(2)\ \mu\text{K}$ on the $5s5p\ ^3P_2$ – $5s4d\ ^3D_3$ transition at $2.9\ \mu\text{m}$. Using this transition, we investigate one dimensional polarization gradient cooling of ^{88}Sr atoms, which have simple energy levels without hyperfine structure, down to $0.22(18)\ \mu\text{K}$ or 17 times the recoil temperature. We discuss prospects for continuous generation of ultracold Sr atoms combined with a state transfer technique.

DOI: [10.1103/PhysRevA.103.023331](https://doi.org/10.1103/PhysRevA.103.023331)

I. INTRODUCTION

Efficient creation of ultracold alkaline-earth-metal(-like) atoms is of significant importance in the development of atomic clocks [1–6] and interferometers [7–10]. Two-stage laser cooling [11–16] on the 1S_0 – 1P_1 and 1S_0 – 3P_1 transitions has been successfully demonstrated for Ca, Sr, Cd, and Yb atoms in the range of a few to sub μK . Reduction of time for obtaining ultracold atoms becomes a serious concern to improve the stability of clocks and interferometers, as the two-stage cooling that requires hundreds of milliseconds inevitably introduces a dead time in the measurements and deteriorates their stabilities via the Dick effect [17]. To overcome the limitations, no-dead-time clock operation has been proposed and demonstrated by combining two atomic clocks [18–21]. Minimally destructive measurement of atomic states with cavity [22,23] has been demonstrated to reduce the loss of ultracold atoms. Repeated imaging of Sr atoms with low loss [24] has been demonstrated in tweezer arrays by implementing Sisyphus cooling to mitigate recoil heating. Interrogation of the clock transition for 15 s [25] has been demonstrated in tweezer arrays, which also leads to high duty cycles of atomic clocks. Continuous generation of ultracold atoms may offer an alternative route to the no-dead-time operation. Simultaneous cooling of ^{88}Sr atoms on the 1S_0 – 1P_1 and 1S_0 – 3P_1 transitions has been demonstrated by spatially separating the cooling regions [26].

The 3P_2 metastable state, having a lifetime of hundreds of seconds [27], allows creation of ultracold atoms using state transfer among long-lived states [28]. Because of its degeneracy, atoms in the 3P_2 state can be cooled to sub-Doppler temperatures [29,30]. Thus far, simultaneous magneto-optical trapping (MOT) on the 1S_0 – 1P_1 and 3P_2 – 3D_3 transitions has been investigated with Ca and Mg atoms [31–33]. Using the infrared 3P_2 – 3D_3 transitions with linewidths of tens of kHz, sub-Doppler cooling down to $20\ \mu\text{K}$ for Ca [31] and Doppler cooling down to $6\ \mu\text{K}$ for Sr [34] have been demonstrated.

In this paper, we investigate laser cooling of Sr atoms on three different transitions starting from the $5s^2\ ^1S_0$ ground state and from the $5s5p\ ^3P_2$ metastable state. We describe a simultaneous MOT of ^{87}Sr atoms on the $5s^2\ ^1S_0$ – $5s5p\ ^1P_1$ transition at 461 nm (blue-MOT; B-MOT) and on the $5s5p\ ^3P_2$ – $5s5d\ ^3D_3$ transition at 496 nm (green-MOT; G-MOT), which is referred to as B/G-MOT. Efficient optical pumping among the hyperfine states in the 3P_2 state and sub-Doppler cooling in the G-MOT improves the transfer efficiency of atoms to the MOT operated on the $5s5p\ ^3P_2$ – $5s4d\ ^3D_3$ transition at $2.9\ \mu\text{m}$ (infrared-MOT; IR-MOT). Moreover, we investigate one-dimensional polarization gradient cooling (PGC) [29,30] of ^{88}Sr atoms on the “IR” transition, where we achieve the lowest temperature of 17 times the photon recoil energy in agreement with recent theories [30,35]. Finally, we discuss prospects for continuous generation of ultracold ^{87}Sr atoms employing three cooling stages.

II. EXPERIMENT

Figure 1(a) shows energy levels for Sr atoms. The “blue” transition ($5s^2\ ^1S_0$ – $5s5p\ ^1P_1$) at 461 nm and the “green” transition ($5s5p\ ^3P_2$ – $5s5d\ ^3D_3$) at 496 nm have natural linewidths of tens of MHz and are conveniently used to cool atoms to less than a mK. The latter transition benefits from sub-Doppler cooling because of the degeneracy in the lower state. The

*Present address: NTT Basic Research Laboratories, Nippon Telegraph and Telephone Corporation, Atsugi, Kanagawa 243-0198, Japan.

†Present address: Gas and Humidity Standards Group, Research Institute for Material and Chemical Measurement, National Metrology Institute of Japan, AIST, Tsukuba, Ibaraki 305-8563, Japan.

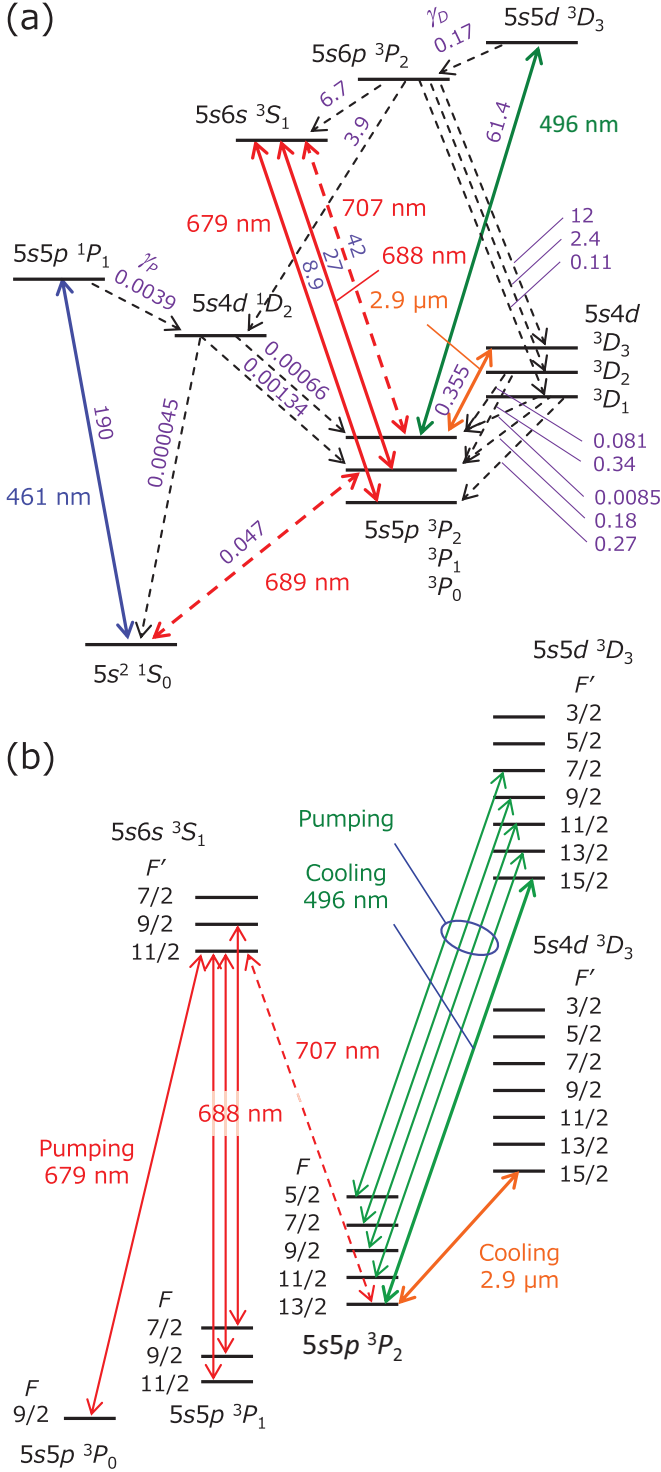


FIG. 1. (a) Relevant energy levels for Sr with the transition decay rates (10^6 s^{-1}). The “blue” (461 nm), “green” (496 nm), and “IR” (2.9 μm) transitions are used for MOT experiments. The transition at 707 nm is used for pumping in the temperature measurement of the G-MOT. (b) Hyperfine structure in the triplet states for ^{87}Sr atoms.

“blue” and “green” transitions have leak channels indicated by dashed lines which allows exchanging atomic populations between the singlet and triplet states, and are used to operate B-MOT and G-MOT simultaneously. The “red”

TABLE I. Properties of the cooling transitions of Sr atoms. λ is the transition wavelength, $\gamma_0/(2\pi)$ natural linewidth, I_0 saturation intensity, a_{max} maximum acceleration, T_D Doppler temperature, T_R recoil temperature, and $\epsilon_R = E_R/(\hbar\gamma_0)$ recoil parameter [35].

Label	“Blue”	“Red”	“Green”	“IR”
Lower state	$5s^2 \ ^1S_0$	$5s^2 \ ^1S_0$	$5s5p \ ^3P_2$	$5s5p \ ^3P_2$
Upper state	$5s5p \ ^1P_1$	$5s5p \ ^3P_1$	$5s5d \ ^3D_3$	$5s4d \ ^3D_3$
λ (nm)	461	689	496	2923
$\gamma_0/(2\pi)$ (Hz)	3.0×10^7	7.5×10^3	9.8×10^6	5.7×10^4
I_0 (mW/cm 2)	40	3.0×10^{-3}	10	3.0×10^{-4}
a_{max} (m/s 2)	9.8×10^5	150	2.8×10^5	270
T_D (μK)	730	0.18	230	1.4
T_R (μK)	0.51	0.23	0.44	0.013
ϵ_R	3.5×10^{-4}	0.64	9.4×10^{-4}	4.7×10^{-3}

transition ($5s^2 \ ^1S_0$ – $5s5p \ ^3P_1$) at 689 nm and the infrared (“IR”) transition ($5s5p \ ^3P_2$ – $5s4d \ ^3D_3$) at 2.9 μm have natural linewidths of 7.5 and 57 kHz, respectively, enabling a low Doppler temperature of a μK , while their natural linewidths provide sufficient scattering force to support atoms against gravity.

Table I summarizes the properties of cooling transitions: Saturation intensity $I_0 = \pi\hbar c\gamma_0/(3\lambda^3)$, maximum acceleration $a_{\text{max}} = \hbar\gamma_0/(2m\lambda)$, Doppler temperature $T_D = \hbar\gamma_0/(2k_B)$, and recoil temperature $T_R = E_R/k_B$ are given for relevant transitions with wavelength λ and natural linewidth $\gamma_0/(2\pi)$. Here c is the speed of light, $\hbar = 2\pi\hbar$ is the Planck constant, k_B is the Boltzmann constant, and $E_R = (\hbar/\lambda)^2/(2m)$ is the photon recoil energy with m the mass of an atom.

Because of nearly an order of magnitude longer wavelength than the visible one, the “IR” transition benefits from a significantly lower recoil temperature of 13 nK that can be approached by sub-Doppler cooling. Generally, laser cooling of atoms can be characterized by the recoil parameter $\epsilon_R = E_R/(\hbar\gamma_0)$, where quantum treatment becomes more relevant for larger ϵ_R [36,37]. It is noteworthy that the recoil parameter $\epsilon_R = 4.7 \times 10^{-3}$ for the “IR” transition is close to the crossover regime where the sub-Doppler cooling mechanism coexists with Doppler cooling [30,35]. Our experiment can be used as a sensitive test of the theory.

Here we mainly discuss the fermionic ^{87}Sr isotope with nuclear spin $I = 9/2$, which is commonly used in optical lattice clocks [1]. Figure 1(b) depicts the hyperfine structure of the triplet states involved in the cooling and pumping transitions (see Tables II and III in Appendix A). In the last part of this section, we describe the sub-Doppler cooling of ^{88}Sr on the “IR” transition.

A. MOT on the “green” transition

Our experimental setup is similar to one described elsewhere [38]. An atomic beam from an oven at a temperature of $\approx 420^\circ\text{C}$ is decelerated by a Zeeman slower and captured by a B-MOT operated on the $^1S_0(F = 9/2)$ – $^1P_1(F' = 11/2)$ transition at 461 nm with a magnetic field gradient of 4 mT/cm. Decay channels from the 1P_1 state to the $5s5p \ ^3P_{1,2}$ states

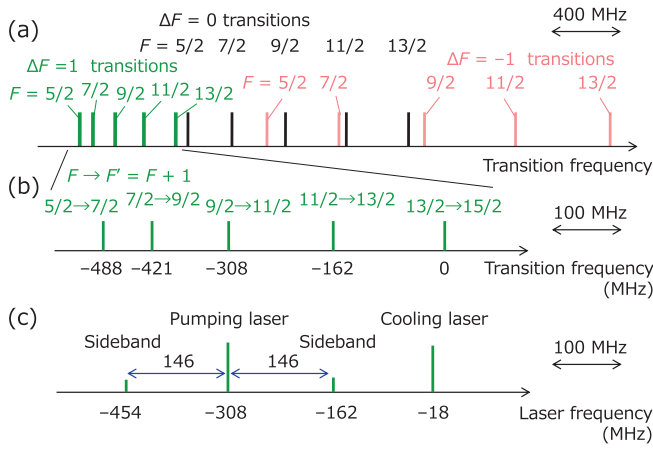


FIG. 2. (a) Frequency diagram of the $5s5p \ ^3P_2(F)$ – $5s5d \ ^3D_3(F')$ transitions at 496 nm for $\Delta F = F' - F = 1, 0$, and -1 , shown in green (dark gray), black, and light red (light gray), respectively. (b) Close view of the frequency diagram of the $\Delta F = 1$ transitions. (c) Schematics of laser frequencies. A cooling laser is tuned to the $F = 13/2 \rightarrow F' = 15/2$ cooling transition. A pumping laser frequency-modulated at 146 MHz resonantly excites $\Delta F = 1$ transitions starting from $F = 5/2, 7/2, 9/2$ and $11/2$ hyperfine states within 35 MHz. The line length represents the optical power ratio, and the sideband power is 30% of the carrier.

via the $5s4d \ ^1D_2$ state [see Fig. 1(a)] continuously supply atoms to the 3P_2 metastable state during the B-MOT. The G-MOT is simultaneously operated on the $^3P_2(F = 13/2)$ – $5s5d \ ^3D_3(F' = 15/2)$ transition at 496 nm. We apply six cooling beams with an e^{-2} diameter of 1.5 cm and a power of 3 mW each, which corresponds to a total peak intensity of $\approx 2I_0^{(G)}$ with $I_0^{(G)} = 10 \text{ mW/cm}^2$ the saturation intensity of the “green” transition. The typical laser detuning is -18 MHz or $-1.8\gamma_0^{(G)}/(2\pi)$ with $\gamma_0^{(G)}/(2\pi) = 9.8 \text{ MHz}$, the natural linewidth. A “green” laser with a power of 20 mW is obtained by frequency-doubling of a master oscillator and power amplifier (MOPA) system with 150 mW at 992 nm, where we use a periodically poled lithium niobate (PPLN) waveguide and an external cavity diode laser (ECDL) as a master oscillator. We employ two such “green” lasers for the G-MOT and for the pumping as described in the following.

Figure 2(a) shows a frequency diagram of $^3P_2(F)$ – $5s5d \ ^3D_3(F')$ transitions where $\Delta F = F' - F = 1, 0$, and -1 transitions are indicated by green (dark gray), black, and light red (light gray) lines (see Tables II and III in Appendix A). The $\Delta F = 1$ transitions are enlarged in Fig. 2(b). To optically pump atomic populations into the $F = 13/2$ state, we frequency-modulate the “green” pumping laser at 146 MHz as shown in Fig. 2(c), where the carrier excites the $F = 9/2 \rightarrow F' = 11/2$ transition and its sidebands excite the $F = 5/2 \rightarrow F' = 7/2$, $F = 7/2 \rightarrow F' = 9/2$, and $F = 11/2 \rightarrow F' = 13/2$ transitions. The sideband power is 30% of the carrier. Thanks to the relatively small spacing of the $\Delta F = 1$ transitions, the sidebands are conveniently generated by current modulation of an ECDL, which is in contrast to the other pumping transitions [34,39] that show hyperfine spacing of more than 1 GHz and require an electro-optic modula-

tor with high-bandwidth. Because the cooling and pumping lasers are detuned by more than 80 MHz from the $\Delta F = 0$ transitions and by more than 457 MHz from the $\Delta F = -1$ transitions, excitation of these transitions is less likely than that of $\Delta F = 1$ transitions. In future experiments, we expect that the cooling and pumping transitions can be covered by a single green-diode-laser by utilizing second-order sidebands with current modulation at 146 MHz.

We note that the G-MOT transition has relatively large branching loss channels. The $5s5d \ ^3D_3$ state has a branching decay rate of $1.7 \times 10^5 \text{ s}^{-1}$ [40] to the $5s6p \ ^3P_2$ state [see Fig. 1(a)], where further decay paths to the $5s5p \ ^3P_{0,1,2}$ states via the $5s4d \ ^1D_2$, $5s6s \ ^3S_1$, and $5s4d \ ^3D_{1,2,3}$ states exist. Atoms decayed to the $^3P_{0,1}$ states are lost from the cooling cycle, which limits the G-MOT lifetime to less than 1 ms. To extend the G-MOT lifetime, we apply four pumping lasers resonant to the $^3P_0(F = 9/2)$ – $5s6s \ ^3S_1(F' = 11/2)$ transition at 679 nm and the $^3P_1(F = 7/2, 9/2, 11/2)$ – $5s6s \ ^3S_1(F' = 9/2 \text{ or } 11/2)$ transitions at 688 nm [41] as shown by red arrows in Fig. 1(b).

Figures 3(a) and 3(b) show the number of atoms N_B in the B-MOT and N_G in the G-MOT, evaluated by fluorescence intensities on the “blue” and “green” transitions, respectively. We start operation of both the B-MOT and the G-MOT at $t = 0 \text{ s}$. While we apply the pumping laser at 679 nm throughout, we turn on three pumping lasers at 688 nm at different times $t = 0$ – 0.6 s as indicated by different colors as shown in the legend. In the absence of the pumping lasers at 688 nm, atoms are mostly trapped by the B-MOT as shown by a red line (A) in Fig. 3(a). The atom loading rate into the B-MOT is $\phi_B = \left. \frac{dN_B}{dt} \right|_{t=0} = 6 \times 10^6 \text{ s}^{-1}$. The number of atoms N_B increases to 1.7×10^6 in 0.6 s.

Applying three pumping lasers at 688 nm at $t = 0 \text{ s}$, the number of atoms N_G in the G-MOT increases with the loading rate $\phi_G = \left. \frac{dN_G}{dt} \right|_{t=0} = 3 \times 10^6 \text{ s}^{-1}$ and reaches an equilibrium value of $\bar{N}_G \approx 6.5 \times 10^5$ as shown by a blue line (B) in Fig. 3(b). We will discuss later that about 40% of atoms stay dark in the 1D_2 state during the B/G-MOT as shown by an orange dashed line in Fig. 3(c).

When the pumping lasers are turned on at $t = 0.6 \text{ s}$, N_G temporarily increases up to 8×10^5 and then relaxes to $\bar{N}_G \approx 6.5 \times 10^5$ as shown by a red line (C) in Fig. 3(b). Such transient response is more pronounced for smaller detuning for the G-MOT as shown in Fig. 9 in Appendix B. This indicates larger light-assisted collisional loss [42,43] in the G-MOT than that in the B-MOT, which is attributed to the lower temperature and higher density in the G-MOT.

The transfer rate of atoms from the B-MOT to the G-MOT is $\phi_{B \rightarrow G} = 3 \times 10^8 \text{ s}^{-1}$ at maximum and it takes 5 ms for N_G to increase to 90% of the maximum value. In the presence of the aforementioned four pumping lasers, the transfer rate is mainly given by the leak rate of $f_P \gamma_P = 390 \text{ s}^{-1}$ where $\gamma_P = 3900 \text{ s}^{-1}$ [40] is the decay rate from the $5s5p \ ^1P_1$ state to the $5s4d \ ^1D_2$ state and $f_P = 0.1$ is the excited atom fraction in the $5s5p \ ^1P_1$ state in the B-MOT for a laser intensity of $2I_0^{(B)}$ at a detuning of -40 MHz or $-1.3\gamma_0^{(B)}/(2\pi)$ with $\gamma_0^{(B)}/(2\pi) = 30 \text{ MHz}$.

After loading atoms into the G-MOT, we turn off the B-MOT to measure the G-MOT lifetime. Figure 4(a) shows

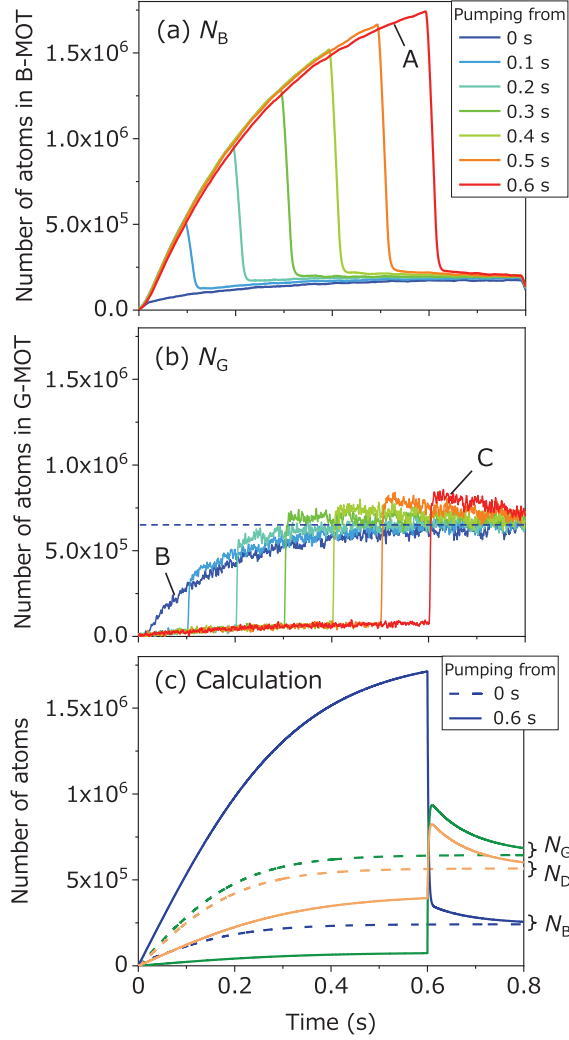


FIG. 3. Number of atoms (a) N_B in the B-MOT and (b) N_G in the G-MOT, simultaneously measured after turning on both MOTs at $t = 0$ s. The color corresponds to timing where the pumping lasers at 688 nm are turned on at $t = 0$ (blue), 0.1, 0.2, 0.3, 0.4, 0.5, and 0.6 s (red) as indicated in the legend. Each N_B (N_G) decreases (increases) rapidly at the timing. A dashed line denotes the equilibrium atom number of $\bar{N}_G = 6.5 \times 10^5$. (c) Calculated number of atoms in B-MOT (N_B : blue lines), G-MOT (N_G : green lines), and in the $5s4d \ ^1D_2$ state (N_D : orange lines) with the pumping lasers from 0 s (dashed lines) and 0.6 s (solid lines).

the number of atoms N_G in the G-MOT operated with laser detunings of -27 MHz to -9 MHz, indicated by different colors as shown in the legend. Figure 4(b) summarizes the lifetime as a function of the laser detuning. For a laser detuning of about -18 MHz or $-1.8\gamma_0^{(G)}/(2\pi)$ we observe the maximum lifetime of 13 ms, which is mainly limited by the available pumping-laser power. We apply three pumping lasers at 688 nm with an e^{-2} diameter of 1 cm and a power of ≈ 0.5 mW each, which corresponds to $\Omega_{\text{pump}}^2 \approx 0.15\gamma_{\text{pump}}^2$ where Ω_{pump} is a Rabi frequency and $\gamma_{\text{pump}} = 2.7 \times 10^7 \text{ s}^{-1}$ is the decay rate of the $5s5p \ ^3P_1 - 5s6s \ ^3S_1$ transition. The leak rate from the cooling cycle is given by $f_D\gamma_D = 1.1 \times 10^4 \text{ s}^{-1}$ where

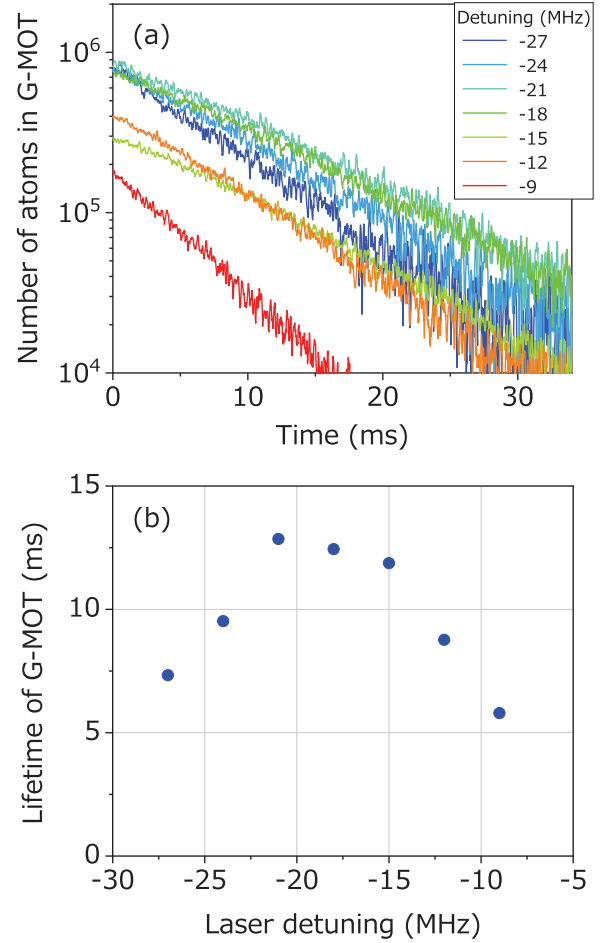


FIG. 4. (a) Number of atoms N_G trapped in the G-MOT after turning off the B-MOT. The color corresponds to detuning of the cooling laser at 496 nm as indicated in the legend. The lines from top to bottom at 15 ms correspond to detuning of -21 , -18 , -24 , -27 , -15 , -12 , and -9 MHz. (b) Measured lifetime of the G-MOT as a function of the laser detuning.

$\gamma_D = 1.7 \times 10^5 \text{ s}^{-1}$ [40] is the decay rate from the $5s5d \ ^3D_3$ state to the $5s6p \ ^3P_2$ state and $f_D = 0.063$ is the excited atom fraction in the $5s5d \ ^3D_3$ state in the G-MOT operated with a laser intensity of $2I_0^{(G)}$ at a detuning of -18 MHz. A certain number of atoms decay from the $5s6p \ ^3P_2$ state to the $5s5p \ ^3P_1$ state via several paths [see Fig. 1(a)]. To extend the G-MOT lifetime, the pumping rate from the $5s5p \ ^3P_1$ state to the $5s5p \ ^3P_2$ state must be sufficiently higher than the decay rate to the $5s^2 \ ^1S_0$ state. In addition, atoms decayed from the $5s6p \ ^3P_2$ state to the $5s4d \ ^1D_2$ state stay there for its lifetime of 0.5 ms. The number of atoms N_D in the $5s4d \ ^1D_2$ state increases as the number of atoms N_G in the G-MOT.

We numerically simulate the number of atoms in the B/G-MOT by rate equations using relevant transitions shown in Fig. 1 (see Appendix C). Figure 3(c) shows N_B (blue lines), N_G (green lines), and N_D (orange lines) with the pumping lasers from 0 s (dashed lines) and 0.6 s (solid lines). We apply three parameters, an excitation rate R_{688} and two-body loss rates β'_B and β'_G as described below, to fit the calculation to experimental data. The excitation rate of the

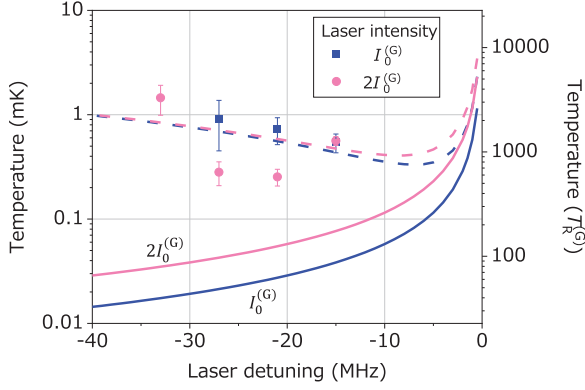


FIG. 5. Temperature of atoms in the G-MOT as a function of the laser detuning for laser intensities of $I_0^{(G)}$ (blue squares) and $2I_0^{(G)}$ (light red circles). Dashed and solid lines show Doppler-cooling temperatures and light shifts, respectively, calculated for laser intensities $I_0^{(G)}$ (blue) and $2I_0^{(G)}$ (light red). The left and right axes show temperatures in units of mK and recoil temperature $T_R^{(G)}$, respectively.

$5s5p\ ^3P_1-5s6s\ ^3S_1$ transition at 688 nm is determined to be $R_{688} = 0.09\gamma_{\text{pump}}$ so that the lifetime of the G-MOT becomes 13 ms. The coefficients for two-body collisional loss in the B-MOT and G-MOT are determined to be $\beta'_B = 2.6 \times 10^{-6}\text{ s}^{-1}$ and $\beta'_G = 1.9 \times 10^{-5}\text{ s}^{-1}$, respectively, so as to reproduce the experimental atom numbers of $N_B \approx 1.7 \times 10^6$ at $t = 0.6\text{ s}$ without the repumping lasers and $N_G \approx 6.5 \times 10^5$ with the repumping lasers.

The temperature of atoms is measured by a time-of-flight (TOF) method. After turning off the B-MOT, we operate the G-MOT for 5 ms, during which we blow away atoms in the 1S_0 ground state by applying a laser resonant to the “blue” transition. Subsequently we turn off the pumping lasers at 688 nm and turn on a pumping laser at 707 nm resonant to the $^3P_2(F = 13/2)-5s6s\ ^3S_1(F' = 11/2)$ transition [see Fig. 1(b)] to transfer the atoms to the 1S_0 state. We measure CCD camera images for different flight times of 1 ms to 10 ms by laser-induced fluorescence (LIF) on the “blue” transition. Figure 5 shows the temperature of atoms as a function of laser detuning with total intensities $I_0^{(G)}$ (blue squares) and $2I_0^{(G)}$ (light red circles) used for the G-MOT. We observe the minimum temperature of 0.25(5) mK for a detuning of -21 MHz or $-2.1\gamma_0^{(G)}/(2\pi)$ with an intensity of $2I_0^{(G)}$.

Atomic temperature expected from the Doppler cooling theory [44] is given by

$$T_{\text{Dop}}(I, \delta) = \frac{\hbar\gamma_0}{4k_B} \frac{I/I_0 + 1 + (2\delta/\gamma_0)^2}{2|\delta|/\gamma_0},$$

where I and $\delta/(2\pi)$ are the intensity and detuning of the cooling laser. Blue and light red dashed lines in Fig. 5 represent $T_{\text{Dop}}^{(G)}(I_0^{(G)}, \delta)$ and $T_{\text{Dop}}^{(G)}(2I_0^{(G)}, \delta)$, respectively. Light shift induced by the cooling laser, which is relevant to PGC temperatures [29,30], is given by

$$U_{\text{dip}}(I, \delta) \approx \frac{a\hbar\gamma_0}{4} \frac{I/I_0}{2|\delta|/\gamma_0},$$

where a is a coefficient depending on the Zeeman substate and the polarization of the laser. Blue and light red solid lines in

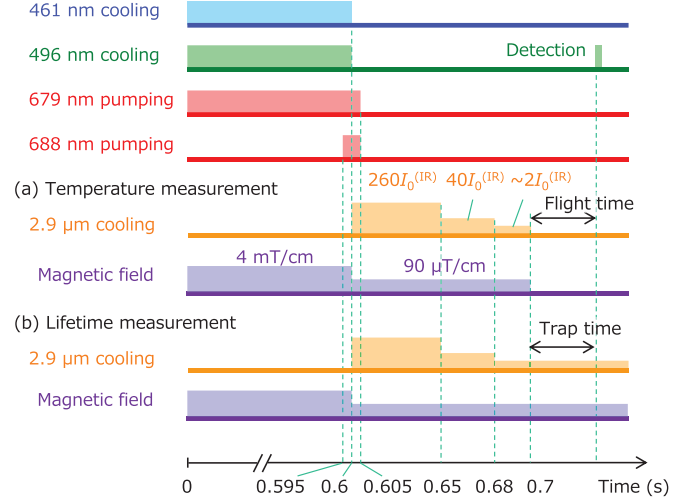


FIG. 6. Timing chart for the IR-MOT. (a) In a temperature measurement, the IR-MOT is turned off at $t = 0.7\text{ s}$ and a velocity distribution of atoms is measured by TOF method. (b) We start a lifetime measurement for the IR-MOT at $t = 0.7\text{ s}$, where atoms reach a steady state temperature for $\approx 2I_0^{(\text{IR})}$.

Fig. 5 represent $U_{\text{dip}}^{(G)}(I_0^{(G)}, \delta)/k_B$ and $U_{\text{dip}}^{(G)}(2I_0^{(G)}, \delta)/k_B$, where we take $a \approx 1$. The measured temperatures (light red circles) are lower than the Doppler temperatures (dashed lines), suggesting PGC works in the G-MOT. The results are consistent with the calculation for $\epsilon_R = 10^{-3}$ in $\sigma_+ - \sigma_-$ configuration [35], where sub-Doppler temperature is obtained for light shifts $U_{\text{dip}} > 100E_R$ and at detunings $|\delta| > 2\gamma_0$ while the atomic temperature diverges for smaller light shifts.

B. MOT with the “IR” transition

After cooling atoms in the G-MOT, we transfer atoms to the IR-MOT operated on the $^3P_2(F = 13/2)-5s4d\ ^3D_3(F' = 15/2)$ transition at $2.9\ \mu\text{m}$. “IR” cooling light with a maximum power of 3.6 mW and a linewidth $\approx 200\text{ Hz}$ is obtained by difference frequency generation from two cavity-stabilized lasers [38]. Figure 6 depicts a timing chart for the cooling sequence. First, we operate the B-MOT and G-MOT simultaneously for 0.6 s without applying the pumping lasers at 688 nm to accumulate atoms in the B-MOT which is less affected by inelastic light-assisted collisions [42,43]. At the end of this process ($t = 0.595\text{ s}$), the pumping lasers at 688 nm are turned on to transfer the atoms to the G-MOT, which increases atom number N_G as shown by the red line (C) in Fig. 3(b). While we turn off the B-MOT and G-MOT at $t = 0.6\text{ s}$, all pumping lasers remain on for another 5 ms to pump atoms in the 1D_2 state to the 3P_2 state. We then operate the IR-MOT by reducing the magnetic field gradient from 4 mT/cm to 90 $\mu\text{T/cm}$ with a total intensity of $260I_0^{(\text{IR})}$ with $I_0^{(\text{IR})} = 0.3\ \mu\text{W/cm}^2$. We reduce the light intensity to $\approx 2I_0^{(\text{IR})}$ in 80 ms and keep this intensity for 20 ms to cool the atoms. The “IR” light and the magnetic field are then turned off at $t = 0.7\text{ s}$ to measure the temperature of atoms by TOF as shown in Fig. 6(a). CCD camera images of atoms in the

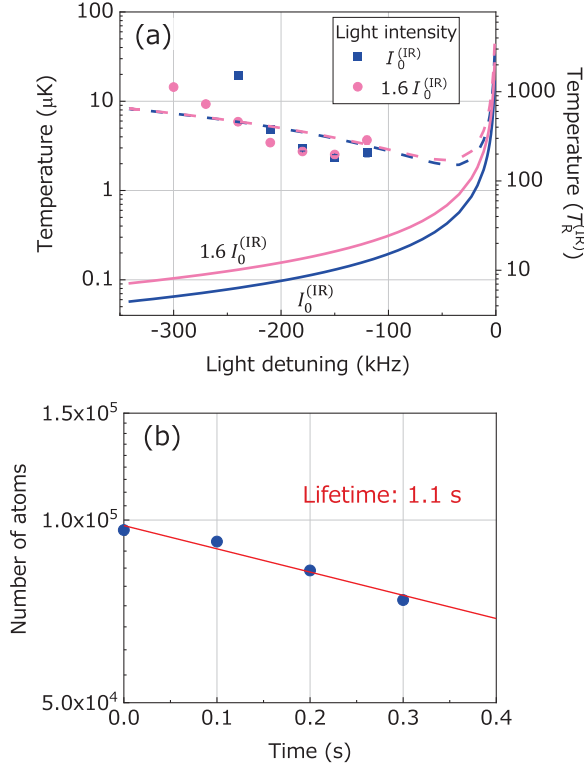


FIG. 7. (a) Temperature of atoms in the IR-MOT as a function of the detuning for light intensities of $I_0^{(\text{IR})}$ (blue squares) and $1.6I_0^{(\text{IR})}$ (light red circles). Dashed and solid lines indicate Doppler-cooling temperatures and light shifts, respectively, calculated for light intensities of $I_0^{(\text{IR})}$ (blue) and $1.6I_0^{(\text{IR})}$ (light red). (b) Number of atoms trapped in the IR-MOT for a detuning of -170 kHz and a light intensity of $1.6I_0^{(\text{IR})}$. A red line shows an exponential decay with a lifetime of 1.1 s.

3P_2 state are observed using LIF on the “green” transition at 496 nm after flight times of 10 and 30 ms.

Figure 7(a) shows the temperature of atoms in the IR-MOT as a function of the detuning from -350 kHz to -100 kHz for light intensities of $I_0^{(\text{IR})}$ (blue squares) and $1.6I_0^{(\text{IR})}$ (light red circles). We observe the minimum temperature of $2.5(2) \mu\text{K}$ at a detuning of -150 kHz or $-2.6\gamma_0^{(\text{IR})}$ with $\gamma_0^{(\text{IR})}/(2\pi) = 57$ kHz [45]. This is lower than the Doppler-cooling temperature $T_{\text{Dop}}^{(\text{IR})}$ [44] calculated for laser intensities of $I_0^{(\text{IR})}$ and $1.6I_0^{(\text{IR})}$, which are shown by blue and light red dashed lines, respectively. Light shifts $U_{\text{dip}}^{(\text{IR})}/k_B$ calculated for $I_0^{(\text{IR})}$ and $1.6I_0^{(\text{IR})}$ are shown by blue and light red solid lines, respectively. The minimum temperature is obtained with $U_{\text{dip}} \approx 15E_R$. This is consistent with the theory [35], where the sub-Doppler cooling becomes less effective as the recoil parameter ϵ_R increases.

A typical number of atoms in the IR-MOT is limited to $N_{\text{IR}} = 1 \times 10^5$, which is achieved for $N_G \approx 4 \times 10^5$ just before transferring atoms from the G-MOT to the IR-MOT. Further increase in N_{IR} is not observed by further increasing $N_G > 4 \times 10^5$, which may be attributed to larger light-assisted collisional loss in the IR-MOT than that in the G-MOT due to the larger scattering cross section on the “IR” transition

in addition to the lower temperature. The maximum transfer efficiency of atoms from the B-MOT with a few mK to the IR-MOT with $2.5 \mu\text{K}$ is 13% . This efficiency is similar to that obtained in the earlier work [34], where the G-MOT is not used and the atomic temperature in the IR-MOT is $6 \mu\text{K}$.

Figure 7(b) shows the lifetime of the IR-MOT operated at a detuning of -170 kHz or $-3\gamma_0^{(\text{IR})}/(2\pi)$ with total light intensity $1.6I_0^{(\text{IR})}$. In this measurement, the IR-MOT is continued as shown in Fig. 6(b), and an exponential decay of the number of atoms from $t = 0.7$ s is recorded. The lifetime of the IR-MOT is measured to be 1.1 s, which is mainly limited by collisions with the background thermal gas at a vacuum pressure of 4×10^{-7} Pa. The off-resonant excitation rate of the $F = 13/2 \rightarrow F' = 13/2$ transition by the cooling light with an intensity of $I_0^{(\text{IR})}$ is estimated to be $2 \times 10^{-4} \text{ s}^{-1}$, which is 4 orders of magnitude smaller than the observed trap decay rate.

C. PGC with the “IR” transition

We investigate one-dimensional PGC on the “IR” transition. In this experiment, we use ^{88}Sr atoms with nuclear spin $I = 0$ to simplify the experiment. Atoms are cooled down to a few μK by a two-stage MOT on the $^1S_0 - ^1P_1$ and $^1S_0 - ^3P_1$ transitions [11], which are then transferred to the 3P_2 state by applying pumping lasers at 688 and 679 nm for 5 ms. We turn off the pumping lasers and zero the magnetic field to be less than $1 \mu\text{T}$ at $t' = 0$, followed by applying counterpropagating “IR” beams with mutually orthogonal linear polarizations at a detuning of -230 kHz or $-4\gamma_0^{(\text{IR})}/(2\pi)$ in the vertical direction, as shown in Fig. 8(a). After shining “IR” beams for 30 ms, we measure atomic temperature in the vertical direction by TOF. Figures 8(b) and 8(c) show TOF images of atoms observed at $t' = 35$ ms and 60 ms with and without “IR” light, where we apply light intensity of $1.7I_0^{(\text{IR})}$ that corresponds to a potential depth of $\approx 0.13 \mu\text{K}$. Atomic distributions in the vertical direction are shown in Fig. 8(d), where blue and light red lines correspond to with and without “IR” light, respectively.

We vary the intensity from $0.07I_0^{(\text{IR})}$ to $13I_0^{(\text{IR})}$, corresponding to potential depths from 5 nK to $1.0 \mu\text{K}$ and estimate the atomic temperature using the atomic distributions at $t' = 35$ ms and 60 ms. Figure 8(e) shows the atomic temperature in the vertical direction as a function of the potential depth $U_{\text{dip}}^{(\text{IR})}(I, \delta)$, where we apply $a = 14/15$ for the $m_J = 2$ substate. Atomic temperature decreases as the potential depth $U_{\text{dip}}^{(\text{IR})}/k_B$. For a potential depth of $0.13 \mu\text{K}$, we obtain the lowest temperature of $0.22(18) \mu\text{K}$ that is 6 times lower than the Doppler temperature of $T_D^{(\text{IR})} = 1.4 \mu\text{K}$. In terms of the recoil energy $E_R^{(\text{IR})}/k_B = 13$ nK, the lowest energy of $17(14)E_R^{(\text{IR})}$ is achieved for the potential depth of $10E_R^{(\text{IR})}$. This result is in contrast with well-known PGC with a small recoil parameter $\epsilon_R < 10^{-3}$, where the atomic energy $k_B T$ is determined by a fraction of the optical potential depth U_{dip} and rapidly increases for the potential depth lower than $\approx 50E_R$ [35]. Our observation for the “IR” transition with $\epsilon_R = 4.7 \times 10^{-3}$ agrees with a theory calculated for a large recoil parameter $\epsilon_R = 10^{-2}$ [35], where sub-Doppler cooling becomes coexistent with Doppler cooling ($\epsilon_R > 10^{-1}$) to keep

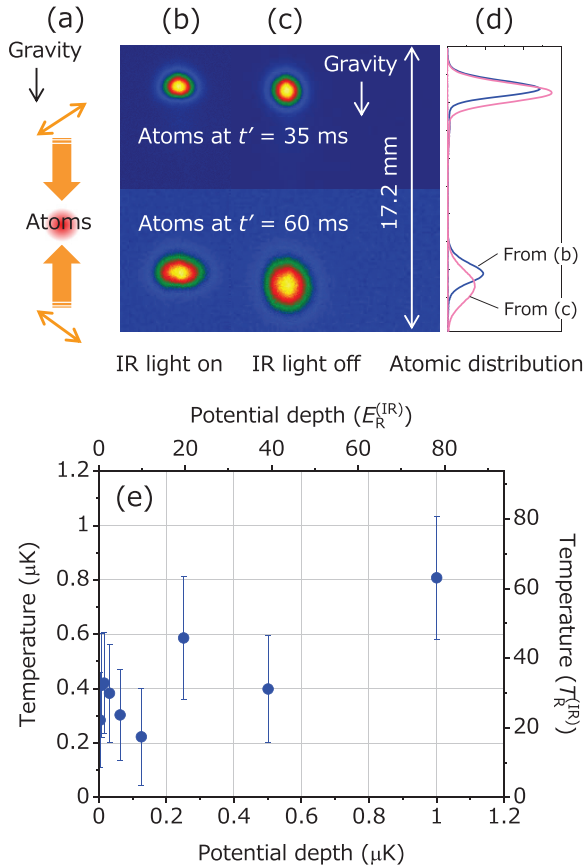


FIG. 8. (a) Configuration of IR beams applied for 30 ms in the vertical direction. Panels (b) and (c) show CCD camera images of atoms at $t' = 35$ ms and 60 ms with and without applying the IR light. (d) Atomic distribution in the vertical direction with (without) the IR light is shown by a blue (light red) line. (e) Temperature of atoms as a function of the potential depth $U_{\text{dip}}^{(\text{IR})}/k_B$.

atomic temperature almost constant for lower optical potential depth.

III. SUMMARY AND OUTLOOK

We have demonstrated simultaneous magneto-optical trapping (B/G-MOT) of ^{87}Sr atoms on the “blue” and “green” transitions. The frequency modulated pumping laser on the “green” transition effectively pumps atoms to the $5s5p\ ^3P_2(F = 13/2)$ state. Thanks to the sub-Doppler temperature of 0.25(5) mK attained in the G-MOT, the simultaneous B/G-MOT improved transfer efficiency of atoms into the IR-MOT operated on the $5s5p\ ^3P_2(F = 13/2)$ – $5s4d\ ^3D_3(F' = 15/2)$ transition at 2.9 μm . Approximately 10^5 atoms are transferred to the IR-MOT, where we observe a trap lifetime of 1.1 s and an atomic temperature of 2.5(2) μK . In addition, we have investigated one-dimensional polarization gradient cooling of ^{88}Sr atoms on the “IR” transition down to a temperature of 0.22(18) μK , which agrees with recent theories.

Thanks to the hyperfine splittings of about 150 MHz in the $5s5p\ ^3P_2(F)$ – $5s5d\ ^3D_3(F' = F + 1)$ transitions, repumping of the hyperfine states in the $5s5p\ ^3P_2$ state during G-MOT is conveniently performed by current modulation of an ECDL.

In future experiments, a single green-diode-laser will cover the cooling and pumping transitions by using second-order sidebands.

Sub-Doppler temperature achieved in the G-MOT facilitates continuous transfer of atoms to a spatially separated [26] IR-MOT with higher efficiency, which can be conveniently applied to construct continuous optical lattice clocks. Optical pumping of atoms from the IR-MOT to the 1S_0 or 3P_0 state permits continuous loading of the atoms into a moving optical lattice [32,46] to transport atoms to a spectroscopy region. It is worth mentioning that the light shift induced by the IR cooling light with an intensity of $I_0^{(\text{IR})}$ is estimated to be as small as $-12\ \mu\text{Hz}$, corresponding to the fractional clock shift of -3×10^{-20} on the $5s^2\ ^1S_0$ – $5s5p\ ^3P_0$ transition. This allows simultaneous operation of the clock and IR-cooling at the same position, offering an opportunity for designing optical lattice clocks.

ACKNOWLEDGMENTS

We thank T. Takano and K. Okamura for their contributions to the experiments in the early stage, and A. Hinton for careful readings of the manuscript and valuable comments. This work was supported by JST ERATO Grant No. JPMJER1002, by JSPS Grant-in-Aid for Specially Promoted Research Grant No. JP16H06284, and by JST-Mirai Program Grant No. JPMJMI18A1, Japan.

APPENDIX A: TRANSITION PROPERTIES

Table II summarizes the magnetic-dipole and electric-quadrupole coupling constants for the $5s5p\ ^3P_2$, $5s5d\ ^3D_3$, and $5s4d\ ^3D_3$ states of ^{87}Sr [47–49]. Table III shows the relative transition frequencies between the $^3P_2(F)$ and $^3D_3(F')$ states in the “green” and “IR” transitions, where we take $F = 13/2$ – $F' = 15/2$ transition frequencies to be zero.

APPENDIX B: G-MOT WITH SMALL DETUNINGS

Two-body collisional loss is pronounced by operating the G-MOT with small detunings that reduce the trap size and increase the atom density. Figures 9(a) and 9(b) show the number of atoms in the G-MOT operated at detunings of -12 MHz and -15 MHz, respectively, with a laser intensity of $2I_0^{(\text{G})}$. As atoms are confined more tightly in the G-MOT for smaller detuning, the equilibrium atom number becomes less due to the two-body collisional loss.

TABLE II. Magnetic-dipole coupling constant A and electric-quadrupole coupling constant B of the $5s5p\ ^3P_2$, $5s5d\ ^3D_3$, and $5s4d\ ^3D_3$ states of ^{87}Sr atoms.

State	A (MHz)	B (MHz)	Ref.
$5s5p\ ^3P_2$	$-212.765(1)$	$67.215(15)$	[47]
$5s5d\ ^3D_3$	$-156.9(3)$	$0(30)$	[48]
$5s4d\ ^3D_3$	$-115.3(2)$	$51(9)$	[49]

TABLE III. Transition frequencies between the $5s5p\ ^3P_2(F)$ and $^3D_3(F')$ states in MHz, calculated from the A and B constants listed in Table II. Relative frequencies in respect to the $F = 13/2 - F' = 15/2$ transitions are presented.

$F-F'$	$^3P_2-5s5d\ ^3D_3$	$^3P_2-5s4d\ ^3D_3$
13/2-11/2	2194	1587
11/2-9/2	1728	880
9/2-7/2	1265	238
7/2-5/2	836	-325
5/2-3/2	439	-800
13/2-13/2	1169	844
11/2-11/2	861	241
9/2-9/2	558	-291
7/2-7/2	286	-740
5/2-5/2	62	-1099
13/2-15/2	0	0
11/2-13/2	-162	-503
9/2-11/2	-308	-929
7/2-9/2	-421	-1269
5/2-7/2	-488	-1514

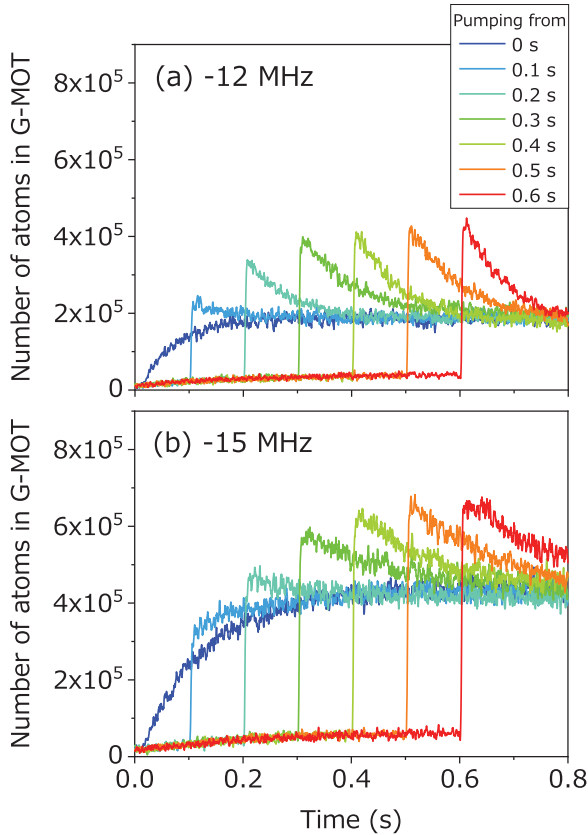


FIG. 9. Number of atoms in the G-MOT operated at a laser detuning of (a) -12 MHz and (b) -15 MHz with a laser intensity of $2I_0^{(G)}$. The color corresponds to timing where the pumping lasers at 688 nm are turned on at $t = 0$ (blue), 0.1, 0.2, 0.3, 0.4, 0.5, and 0.6 s (red). Each number of atoms increases rapidly at the timing.

APPENDIX C: RATE EQUATIONS

The rate equations for the relevant states shown in Fig. 1(a) are given by

$$\begin{aligned} \frac{dN_{1S_0}}{dt} &= \phi_{\text{oven}} + \gamma_{1P_1 \rightarrow 1S_0} N_{1P_1} + \gamma_{1D_2 \rightarrow 1S_0} N_{1D_2} \\ &\quad + \gamma_{3P_1 \rightarrow 1S_0} N_{3P_1} - R_{461} (N_{1S_0} - N_{1P_1}) \\ &\quad - \beta'_B N_{1S_0}^2, \end{aligned}$$

$$\begin{aligned} \frac{dN_{1P_1}}{dt} &= R_{461} (N_{1S_0} - N_{1P_1}) \\ &\quad - (\gamma_{1P_1 \rightarrow 1S_0} + \gamma_{1P_1 \rightarrow 1D_2}) N_{1P_1}, \end{aligned}$$

$$\begin{aligned} \frac{dN_{1D_2}}{dt} &= \gamma_{1P_1 \rightarrow 1D_2} N_{1P_1} + \gamma_{6P\ ^3P_2 \rightarrow 1D_2} N_{6P\ ^3P_2} \\ &\quad - (\gamma_{1D_2 \rightarrow 1S_0} + \gamma_{1D_2 \rightarrow 3P_2} + \gamma_{1D_2 \rightarrow 3P_1}) N_{1D_2}, \end{aligned}$$

$$\begin{aligned} \frac{dN_{3S_1}}{dt} &= \gamma_{6P\ ^3P_2 \rightarrow 3S_1} N_{6P\ ^3P_2} + R_{688} (N_{3P_1} - N_{3S_1}) \\ &\quad + R_{679} (N_{3P_0} - N_{3S_1}) \\ &\quad - (\gamma_{3S_1 \rightarrow 3P_2} + \gamma_{3S_1 \rightarrow 3P_1} + \gamma_{3S_1 \rightarrow 3P_0}) N_{3S_1}, \end{aligned}$$

$$\begin{aligned} \frac{dN_{3P_2}}{dt} &= \gamma_{1D_2 \rightarrow 3P_2} N_{1D_2} + \gamma_{3S_1 \rightarrow 3P_2} N_{3S_1} \\ &\quad + \gamma_{5d\ ^3D_3 \rightarrow 3P_2} N_{5d\ ^3D_3} + \gamma_{3D_3 \rightarrow 3P_2} N_{3D_3} \\ &\quad + \gamma_{3D_2 \rightarrow 3P_2} N_{3D_2} + \gamma_{3D_1 \rightarrow 3P_2} N_{3D_1} \\ &\quad - R_{496} (N_{3P_2} - N_{5d\ ^3D_3}) - \beta'_G N_{3P_2}^2, \end{aligned}$$

$$\begin{aligned} \frac{dN_{3P_1}}{dt} &= \gamma_{1D_2 \rightarrow 3P_1} N_{1D_2} + \gamma_{3S_1 \rightarrow 3P_1} N_{3S_1} \\ &\quad + \gamma_{3D_2 \rightarrow 3P_1} N_{3D_2} + \gamma_{3D_1 \rightarrow 3P_1} N_{3D_1} \\ &\quad - R_{688} (N_{3P_1} - N_{3S_1}) - \gamma_{3P_1 \rightarrow 1S_0} N_{3P_1}, \end{aligned}$$

$$\begin{aligned} \frac{dN_{3P_0}}{dt} &= \gamma_{3S_1 \rightarrow 3P_0} N_{3S_1} + \gamma_{3D_1 \rightarrow 3P_0} N_{3D_1} \\ &\quad - R_{679} (N_{3P_0} - N_{3S_1}), \end{aligned}$$

$$\begin{aligned} \frac{dN_{6P\ ^3P_2}}{dt} &= \gamma_{5d\ ^3D_3 \rightarrow 6P\ ^3P_2} N_{5d\ ^3D_3} \\ &\quad - (\gamma_{6P\ ^3P_2 \rightarrow 1D_2} + \gamma_{6P\ ^3P_2 \rightarrow 3S_1} + \gamma_{6P\ ^3P_2 \rightarrow 3D_3} \\ &\quad + \gamma_{6P\ ^3P_2 \rightarrow 3D_2} + \gamma_{6P\ ^3P_2 \rightarrow 3D_1}) N_{6P\ ^3P_2}, \end{aligned}$$

$$\frac{dN_{3D_3}}{dt} = \gamma_{6P\ ^3P_2 \rightarrow 3D_3} N_{6P\ ^3P_2} - \gamma_{3D_3 \rightarrow 3P_2} N_{3D_3},$$

$$\begin{aligned} \frac{dN_{3D_2}}{dt} &= \gamma_{6P\ ^3P_2 \rightarrow 3D_2} N_{6P\ ^3P_2} \\ &\quad - (\gamma_{3D_2 \rightarrow 3P_2} + \gamma_{3D_2 \rightarrow 3P_1}) N_{3D_2}, \end{aligned}$$

$$\begin{aligned} \frac{dN_{3D_1}}{dt} &= \gamma_{6P\ ^3P_2 \rightarrow 3D_1} N_{6P\ ^3P_2} \\ &\quad - (\gamma_{3D_1 \rightarrow 3P_2} + \gamma_{3D_1 \rightarrow 3P_1} + \gamma_{3D_1 \rightarrow 3P_0}) N_{3D_1}, \end{aligned}$$

$$\begin{aligned} \frac{dN_{5d\ ^3D_3}}{dt} &= R_{496} (N_{3P_2} - N_{5d\ ^3D_3}) \\ &\quad - (\gamma_{5d\ ^3D_3 \rightarrow 3P_2} + \gamma_{5d\ ^3D_3 \rightarrow 6P\ ^3P_2}) N_{5d\ ^3D_3}, \end{aligned}$$

TABLE IV. The number of atoms N_k in the state (k) and decay rate $\gamma_{k \rightarrow i}$ from the upper state (k) to the lower state (i).

State	No. of atoms	Decay rate (s ⁻¹)	Ref.
$5s^2 \ ^1S_0$	$N_{^1S_0}$	0	
$5s5p \ ^1P_1$	$N_{^1P_1}$	$\gamma_{^1P_1 \rightarrow ^1S_0}$ $1.900(2) \times 10^8$	[51]
		$\gamma_{^1P_1 \rightarrow ^1D_2}$ $3.9(1.5) \times 10^3$	[40]
$5s4d \ ^1D_2$	$N_{^1D_2}$	$\gamma_{^1D_2 \rightarrow ^1S_0}$ 44.7^a	[52]
		$\gamma_{^1D_2 \rightarrow ^3P_2}$ 661^a	[52]
		$\gamma_{^1D_2 \rightarrow ^3P_1}$ 1.34×10^{3a}	[52]
$5s6s \ ^3S_1$	$N_{^3S_1}$	$\gamma_{^3S_1 \rightarrow ^3P_2}$ $4.2(4) \times 10^7$	[53]
		$\gamma_{^3S_1 \rightarrow ^3P_1}$ $2.7(2) \times 10^7$	[53]
		$\gamma_{^3S_1 \rightarrow ^3P_0}$ $8.9(8) \times 10^6$	[53]
$5s5p \ ^3P_2$	$N_{^3P_2}$	<0.01	[27]
$5s5p \ ^3P_1$	$N_{^3P_1}$	$\gamma_{^3P_1 \rightarrow ^1S_0}$ $4.69(11) \times 10^4$	[54]
$5s5p \ ^3P_0$	$N_{^3P_0}$	<0.01	[55]
$5s6p \ ^3P_2$	$N_{6p \ ^3P_2}$	$\gamma_{6p \ ^3P_2 \rightarrow ^1D_2}$ 3.9×10^{6a}	[40]
		$\gamma_{6p \ ^3P_2 \rightarrow ^3S_1}$ 6.73×10^{6a}	[40]
		$\gamma_{6p \ ^3P_2 \rightarrow ^3D_3}$ 1.2×10^{7a}	[40]
		$\gamma_{6p \ ^3P_2 \rightarrow ^3D_2}$ 2.4×10^{6a}	[40]
		$\gamma_{6p \ ^3P_2 \rightarrow ^3D_1}$ 1.1×10^{5a}	[40]
$5s4d \ ^3D_3$	$N_{^3D_3}$	$\gamma_{^3D_3 \rightarrow ^3P_2}$ $3.55(4) \times 10^5$	[45]
$5s4d \ ^3D_2$	$N_{^3D_2}$	$\gamma_{^3D_2 \rightarrow ^3P_{1,2}}$ $4.16(5) \times 10^5$	[45]
$5s4d \ ^3D_1$	$N_{^3D_1}$	$\gamma_{^3D_1 \rightarrow ^3P_{0,1,2}}$ $4.61(5) \times 10^5$	[45]
$5s5d \ ^3D_3$	$N_{5d \ ^3D_3}$	$\gamma_{5d \ ^3D_3 \rightarrow 6p \ ^3P_2}$ 1.7×10^{5a}	[40]
		$\gamma_{5d \ ^3D_3 \rightarrow ^3P_2}$ $6.14(9) \times 10^7$	[53]

^aUncertainties are not estimated.

^bFine-structure branching ratios are calculated using the 6- j symbols for the rate equations and Fig. 1(a).

where N_k denotes the number of atoms in the state (k) and $\gamma_{k \rightarrow i}$ denotes the decay rate from the upper state (k) to the lower state (i). We list N_k and $\gamma_{k \rightarrow i}$ in Table IV. In the main text, $\gamma_0^{(B)}$, $\gamma_0^{(G)}$, $\gamma_0^{(IR)}$, γ_P , γ_D , and γ_{pump} indicate $\gamma_{^1P_1 \rightarrow ^1S_0}$, $\gamma_{5d \ ^3D_3 \rightarrow ^3P_2}$, $\gamma_{^3D_3 \rightarrow ^3P_2}$, $\gamma_{^1P_1 \rightarrow ^1D_2}$, $\gamma_{5d \ ^3D_3 \rightarrow 6p \ ^3P_2}$, and $\gamma_{^3S_1 \rightarrow ^3P_1}$, respectively. Figure 3(c) shows the calculation results for $N_B = N_{^1S_0} + N_{^1P_1}$, $N_G = N_{^3P_2} + N_{5d \ ^3D_3}$, and $N_D = N_{^1D_2}$.

We estimate the atom loading rate from the oven is $\phi_{\text{oven}} = 7 \times 10^6 \text{ s}^{-1}$ using ϕ_B and ϕ_G . The excitation rate for a transition with natural linewidth $\gamma_0/(2\pi)$ is given by [38,50]

$$R = \frac{\Omega^2}{\gamma_0} \frac{1}{1 + (2\delta/\gamma_0)^2},$$

where Ω and $\delta/(2\pi)$ are the Rabi frequency and detuning of the applied laser. We set $R_{461} = 0.13\gamma_{^1P_1 \rightarrow ^1S_0}$, $R_{496} = 0.072\gamma_{5d \ ^3D_3 \rightarrow ^3P_2}$, and $R_{679} = 0.054\gamma_{^3S_1 \rightarrow ^3P_0}$ with the detuning and intensity of each laser in the experiment. As the G-MOT life time mainly depends on R_{688} , we determine $R_{688} = 0.09\gamma_{^3S_1 \rightarrow ^3P_1}$ by fitting the G-MOT lifetime to the experimental value of 13 ms. $\beta'_B = 2.6 \times 10^{-6} \text{ s}^{-1}$ and $\beta'_G = 1.9 \times 10^{-5} \text{ s}^{-1}$ denote the coefficients for two-body collisional loss in the B-MOT and G-MOT, determined by fitting the numbers of atoms to the experimental values of $N_B \approx 1.7 \times 10^6$ at $t = 0.6 \text{ s}$ and $\tilde{N}_G \approx 6.5 \times 10^5$, respectively. We neglect the linear loss rate by the back ground gas collision.

- [1] H. Katori, M. Takamoto, V. G. Pal'chikov, and V. D. Ovsiannikov, Ultrastable Optical Clock with Neutral Atoms in an Engineered Light Shift Trap, *Phys. Rev. Lett.* **91**, 173005 (2003).
- [2] R. Le Targat, L. Lorini, Y. Le Coq, M. Zawada, J. Guéna, M. Abgrall, M. Gurov, P. Rosenbusch, D. G. Rovera, B. Nagórny, R. Gartman, P. G. Westergaard, M. E. Tobar, M. Lours, G. Santarelli, A. Clairon, S. Bize, P. Laurent, P. Lemonde, and J. Lodewyck, Experimental realization of an optical second with strontium lattice clocks, *Nat. Commun.* **4**, 2109 (2013).
- [3] S. B. Koller, J. Grotti, S. Vogt, A. Al-Masoudi, S. Dörscher, S. Häfner, U. Sterr, and Ch. Lisdat, Transportable Optical Lattice Clock with 7×10^{-17} Uncertainty, *Phys. Rev. Lett.* **118**, 073601 (2017).
- [4] E. Oelker, R. B. Hutson, C. J. Kennedy, L. Sonderhouse, T. Bothwell, A. Goban, D. Kedar, C. Sanner, J. M. Robinson, G. E. Marti, D. G. Matei, T. Legero, M. Giunta, R. H. and F. Riehle, U. Sterr, and J. Ye, Demonstration of 4.8×10^{-17} stability at 1 s for two independent optical clocks, *Nat. Photonics* **13**, 714 (2019).
- [5] J. Olson, R. W. Fox, T. M. Fortier, T. F. Sheerin, R. C. Brown, H. Leopardi, R. E. Stoner, C. W. Oates, and A. D. Ludlow, Ramsey-Borde Matter-Wave Interferometry for Laser Frequency Stabilization at 10^{-16} Frequency Instability and Below, *Phys. Rev. Lett.* **123**, 073202 (2019).
- [6] W. Bowden, R. Hobson, I. R. Hill, A. Vianello, M. Schioppa, A. Silva, H. S. Margolis, P. E. G. Baird, and P. Gill, A pyramid MOT with integrated optical cavities as a cold atom platform for an optical lattice clock, *Sci. Rep.* **9**, 11704 (2019).
- [7] F. Riehle, T. Kisters, A. Witte, J. Helmcke, and Ch. J. Bordé, Optical Ramsey Spectroscopy in a Rotating Frame: Sagnac Effect in a Matter-Wave Interferometer, *Phys. Rev. Lett.* **67**, 177 (1991).
- [8] G. Ferrari, N. Poli, F. Sorrentino, and G. M. Tino, Long-Lived Bloch Oscillations with Bosonic Sr Atoms and Application to Gravity Measurement at the Micrometer Scale, *Phys. Rev. Lett.* **97**, 060402 (2006).
- [9] T. Akatsuka, T. Takahashi, and H. Katori, Optically guided atom interferometer tuned to magic wavelength, *Appl. Phys. Express* **10**, 112501 (2017).
- [10] L. Hu, N. Poli, L. Salvi, and G. M. Tino, Atom Interferometry with the Sr Optical Clock Transition, *Phys. Rev. Lett.* **119**, 263601 (2017).
- [11] H. Katori, T. Ido, Y. Isoya, and M. Kuwata-Gonokami, Magneto-Optical Trapping and Cooling of Strontium Atoms Down to the Photon Recoil Temperature, *Phys. Rev. Lett.* **82**, 1116 (1999).
- [12] T. Kuwamoto, K. Honda, Y. Takahashi, and T. Yabuzaki, Magneto-optical trapping of Yb atoms using an intercombination transition, *Phys. Rev. A* **60**, R745 (1999).
- [13] T. Binnewies, G. Wilpers, U. Sterr, F. Riehle, J. Helmcke, T. E. Mehlstäubler, E. M. Rasel, and W. Ertmer, Doppler Cooling and Trapping on Forbidden Transitions, *Phys. Rev. Lett.* **87**, 123002 (2001).

- [14] E. A. Curtis, C. W. Oates, and L. Hollberg, Quenched narrow-line laser cooling of ^{40}Ca to near the photon recoil limit, *Phys. Rev. A* **64**, 031403(R) (2001).
- [15] T. Mukaiyama, H. Katori, T. Ido, Y. Li, and M. Kuwata-Gonokami, Recoil-Limited Laser Cooling of ^{87}Sr Atoms Near the Fermi Temperature, *Phys. Rev. Lett.* **90**, 113002 (2003).
- [16] A. Yamaguchi, M. S. Safronova, K. Gibble, and H. Katori, Narrow-Line Cooling and Determination of the Magic Wavelength of Cd, *Phys. Rev. Lett.* **123**, 113201 (2019).
- [17] G. Santarelli, C. Audoin, A. Makdissi, P. Laurent, G. J. Dick, and A. Clairon, Frequency stability degradation of an oscillator slaved to a periodically interrogated atomic resonator, *IEEE Trans. Ultrason. Ferroelectr. Freq. Control* **45**, 887 (1998).
- [18] G. J. Dick, J. D. Prestage, C. A. Greenhall, and L. Maleki, Local oscillator induced degradation of medium-term stability in passive atomic frequency standards, in *Proceedings of the 22th Annual Precise Time and Time Interval Systems and Applications Meeting* (Institute of Navigation, Manassas, VA, 1990), pp. 487–508.
- [19] J. Lodewyck, P. G. Westergaard, A. Lecallier, L. Lorini, and P. Lemonde, Frequency stability of optical lattice clocks, *New J. Phys.* **12**, 065026 (2010).
- [20] G. W. Biedermann, K. Takase, X. Wu, L. Deslauriers, S. Roy, and M. A. Kasevich, Zero-Dead-Time Operation of Interleaved Atomic Clocks, *Phys. Rev. Lett.* **111**, 170802 (2013).
- [21] M. Schioppo, R. C. Brown, W. F. McGrew, N. Hinkley, R. J. Fasano, K. Beloy, T. H. Yoon, G. Milani, D. Nicolodi, J. A. Sherman, N. B. Phillips, C. W. Oates, and A. D. Ludlow, Ultrastable optical clock with two cold-atom ensembles, *Nat. Photonics* **11**, 48 (2017).
- [22] J. Lodewyck, P. G. Westergaard, and P. Lemonde, Nondestructive measurement of the transition probability in a Sr optical lattice clock, *Phys. Rev. A* **79**, 061401(R) (2009).
- [23] G. Vallet, E. Bookjans, U. Eismann, S. Bilicki, R. L. Targat, and J. Lodewyck, A noise-immune cavity-assisted non-destructive detection for an optical lattice clock in the quantum regime, *New J. Phys.* **19**, 083002 (2017).
- [24] J. P. Covey, I. S. Madjarov, A. Cooper, and M. Endres, 2000-times Repeated Imaging of Strontium Atoms in Clock-Magic Tweezer Arrays, *Phys. Rev. Lett.* **122**, 173201 (2019).
- [25] A. W. Young, W. J. Eckner, W. R. Milner, D. Kedar, M. A. Norcia, E. Oelker, N. Schine, J. Ye, and A. M. Kaufman, Half-minute-scale atomic coherence and high relative stability in a tweezer clock, *Nature* **588**, 408 (2020).
- [26] S. Bennetts, C.-C. Chen, B. Pasquiou, and F. Schreck, Steady-State Magneto-Optical Trap with 100-Fold Improved Phase-Space Density, *Phys. Rev. Lett.* **119**, 223202 (2017).
- [27] M. Yasuda and H. Katori, Lifetime measurement of the 3P_2 Metastable state of Strontium Atoms, *Phys. Rev. Lett.* **92**, 153004 (2004).
- [28] H. Katori, T. Ido, Y. Isoya, and M. Kuwata-Gonokami, Laser cooling of strontium atoms toward quantum degeneracy, in *Atomic Physics 17: XVII International Conference on Atomic Physics; ICAP 2000*, edited by P. De Natale, E. Arimondo, and M. Inguscio, AIP Conf. Proc. No. 551 (AIP, New York, 2001), p. 382.
- [29] J. Dalibard and C. Cohen-Tannoudji, Laser cooling below the doppler limit by polarization gradients: Simple theoretical models, *J. Opt. Soc. Am. B* **6**, 2023 (1989).
- [30] O. N. Prudnikov, D. V. Brazhnikov, A. V. Taichenachev, V. I. Yudin, A. E. Bonert, R. Ya. Il'enkov, and A. N. Goncharov, Quantum treatment of two-stage sub-Doppler laser cooling of magnesium atoms, *Phys. Rev. A* **92**, 063413 (2015).
- [31] J. Grünert and A. Hemmerich, Sub-Doppler magneto-optical trap for calcium, *Phys. Rev. A* **65**, 041401(R) (2002).
- [32] C. Y. Yang, P. Halder, O. Appel, D. Hansen, and A. Hemmerich, Continuous loading of 1S_0 calcium atoms into an optical dipole trap, *Phys. Rev. A* **76**, 033418 (2007).
- [33] M. Riedmann, H. Kelkar, T. Wübbena, A. Pape, A. Kulosa, K. Zipfel, D. Fim, S. Rühmann, J. Friebe, W. Ertmer, and E. Rasel, Beating the density limit by continuously loading a dipole trap from millikelvin-hot magnesium atoms, *Phys. Rev. A* **86**, 043416 (2012).
- [34] R. Hobson, W. Bowden, A. Vianello, I. R. Hill, and P. Gill, Midinfrared magneto-optical trap of metastable strontium for an optical lattice clock, *Phys. Rev. A* **101**, 013420 (2020).
- [35] A. A. Kirpichnikova, O. N. Prudnikov, R. Ya Il'enkov, A. V. Taichenachev, and V. I. Yudin, Limits of sub-Doppler cooling for atoms with various recoil parameter, [arXiv:2002.06809v1](https://arxiv.org/abs/2002.06809v1).
- [36] Y. Castin, H. Wallis, and J. Dalibard, Limit of Doppler cooling, *J. Opt. Soc. Am. B* **6**, 2046 (1989).
- [37] H. J. Metcalf and P. van der Straten, *Laser Cooling and Trapping* (Springer-Verlag, New York, 1999).
- [38] K. Hashiguchi, T. Akatsuka, N. Ohmae, M. Takamoto, and H. Katori, Frequency measurement on the $5s5p\ ^3P_2-5s4d\ ^3D_3$ transition of ^{88}Sr atoms using photon momentum transfer technique, *Phys. Rev. A* **100**, 042513 (2019).
- [39] T. Yang, K. Pandey, M. S. Pramod, F. Leroux, C. C. Kwong, E. Hajiyev, Z. Y. Chia, B. Fang, and D. Wilkowski, A high flux source of cold strontium atoms, *Eur. Phys. J. D* **69**, 226 (2015).
- [40] H. G. C. Werij, C. H. Greene, C. E. Theodosiou, and A. Gallagher, Oscillator strengths and radiative branching ratios in atomic Sr, *Phys. Rev. A* **46**, 1248 (1992).
- [41] D. S. Barker, B. J. Reschovsky, N. C. Pienti, and G. K. Campbell, Enhanced magnetic trap loading for atomic strontium, *Phys. Rev. A* **92**, 043418 (2015).
- [42] A. Gallagher and D. E. Pritchard, Exoergic Collisions of Cold Na^*-Na , *Phys. Rev. Lett.* **63**, 957 (1989).
- [43] J. Weiner, V. S. Bagnato, S. Zilio, and P. S. Julienne, Experiments and theory in cold and ultracold collisions, *Rev. Mod. Phys.* **71**, 1 (1999).
- [44] P. D. Lett, W. D. Phillips, S. L. Rolston, E. C. Tanner, R. N. Watts, and C. I. Westbrook, Optical molasses, *J. Opt. Soc. Am. B* **6**, 2084 (1989).
- [45] M. S. Safronova, S. G. Porsev, U. I. Safronova, M. G. Kozlov, and C. W. Clark, Blackbody-radiation shift in the Sr optical atomic clock, *Phys. Rev. A* **87**, 012509 (2013).
- [46] I. Ushijima, M. Takamoto, M. Das, T. Ohkubo, and H. Katori, Cryogenic optical lattice clocks, *Nat. Photonics* **9**, 185 (2015).
- [47] S. M. Heider and G. O. Brink, Hyperfine structure of ^{87}Sr in the 3P_2 metastable state, *Phys. Rev. A* **16**, 1371 (1977).
- [48] S. Stellmer and F. Schreck, Reservoir spectroscopy of $5s5p\ ^3P_2-5snd\ ^3D_{1,2,3}$ transitions in strontium, *Phys. Rev. A* **90**, 022512 (2014).
- [49] B. A. Bushaw, H. J. Kluge, J. Lantzsich, R. Schwalbach, J. Stenner, H. Stevens, K. Wendt, and K. Zimmer, Hyperfine structure in $5s4d\ ^3D-5snf$ transitions of ^{87}Sr , *Z. Phys. D* **28**, 275 (1993).

- [50] J. I. Kim, D. Haubrich, B. Klöter, and D. Meschede, Strong effective saturation by optical pumping in three-level systems, *Phys. Rev. A* **80**, 063801 (2009).
- [51] M. Yasuda, T. Kishimoto, M. Takamoto, and H. Katori, Photoassociation spectroscopy of ^{88}Sr : Reconstruction of the wave function near the last node, *Phys. Rev. A* **73**, 011403(R) (2006).
- [52] C. W. Bauschlicher Jr, S. R. Langhoff, and H. Partridge, The radiative lifetime of the 1D_2 state of Ca and Sr: A core-valence treatment, *J. Phys. B* **18**, 1523 (1985).
- [53] G. García and J. Campos, Transition probabilities for triplet levels of Sr(I), *J. Quant. Spectrosc. Radiat. Transfer* **39**, 477 (1988).
- [54] R. Drozdowski, M. Ignaciuk, J. Kwela, and J. Heldt, Radiative lifetimes of the lowest 3P_1 metastable states of Ca and Sr, *Z. Phys. D* **41**, 125 (1997).
- [55] S. G. Porsev and A. Derevianko, Hyperfine quenching of the metastable $^3P_{0,2}$ states in divalent atoms, *Phys. Rev. A* **69**, 042506 (2004).